Measuring The Urban Heat Island Effect: Does Scale Matter?

Huon Morton, n10753826

Queensland University of Technology (QUT)

EVB203: Geospatial Information Science

EVB203 Assessment 2: Scientific Report

Dr. Catherine Kim

Semester 1, 31 May 2024

Word Count: 2,152

1. Introduction

The Urban Heat Island Effect (UHI) is a very well-documented and dangerous phenomenon, causing temperature spikes within dense urban sprawls which can threaten the health of the public and essential public systems. It has been the focus of many research topics and government initiatives to correctly identify and measure UHIs in high-density urban developments for the benefit of all socioeconomic interests (Lin et al., 2017). The current literature is immense and extensive; however, there is little research on the importance of measurements at different scales, especially with the inclusion of experimental data.

As the human population shows no sign of slowing down, it is of utmost interest to find manageable methods for conducting analyses to support development policies. With an influx of literature, Kim and Brown (2021) conveniently reviewed 51 articles on UHIs to develop a concise summarisation and criticism of the various classification methods for measuring UHIs. This review offered many insights into the most recommended pathways for UHI analysis, mentioning that among the large corpus of information available, there have been little efforts to investigate the causative factors for UHIs and to incorporate experimental data into statistical and predictive models for more precise policy recommendations.

Precision is a major consideration for spatial analysts and is often the most difficult to execute; as a result, most studies analysing UHIs utilise publicly available satellite imagery with low resolutions which may not detect local anomalies (Giannaros et al., 2018; Li et al., 2018). This creates an overabundance of studies that analyse moderate scales which can mask the intricacies associated with UHIs. Thus, this study will comparatively investigate the differences between the statistical analyses of UHIs on a micro-, meso- and macroscale. The micro- and mesoscales will be investigated using publicly available land surface temperature (LST) data

from the Landsat program initiated by NASA and USGS (see Appendix A, Figure A2 and Table A3). Experimental air temperature data will be used to highlight any significant phenomena that may arise due to other atmospheric factors. In addition to this, a recent study analysing the UHI associated with the greater Brisbane area will be used as evidence for the macroscale as the current technology available for this study was unsuitable (Deilami & Kamruzzaman, 2017).

1.1 Aims

Traditionally, UHIs are measured by reference to rural areas outside of the urban sprawl. This study is instead focusing on the suitability for determining contributing UHI factors within given areas at different scales. These findings will aim to provide evidence for the question: Are urban heat island effect factors more suitably detected on a microscale? This will be substantiated through the following hypotheses:

1. Does remote sensing imagery suitably detect differences in land surface temperatures at three different scales of the Brisbane area?

2. Does experimental data produce more accurate and significant differences in air temperature at a microscale in Brisbane City, as opposed to LST remote sensing?

1.2 Classifications

At present, there is no universally agreed standard for scaling, thus it is necessary to state the scales selected in this study. These were classified mostly following the horizontal range generalisations developed by Kim and Brown (2021), excluding the "local" range (Table 1).

Scale	**Microscale**	**Mesoscale**	**Macroscale**
Area (m^2, km^2)	100 m^2 - 0.5 km^2	0.5 km^2 – 100 km^2	100 km^2 <

Table 1. The classification table of area scales referred to throughout the study.

2. Methodology

2.1 Study sites

The boundary for fieldwork extended from the City Botanic Gardens to the Roma Street Parklands in Brisbane City, approximately 2.6 km in length (Figure 1). North Brisbane LST was sourced from the website Earth Explorer, remotely sensed by the NASA and USGS initiated Landsat 8 satellite. The spatial analysis of the greater Brisbane area was sourced from an adjacent study by Deilami and Kamruzzaman (2017).

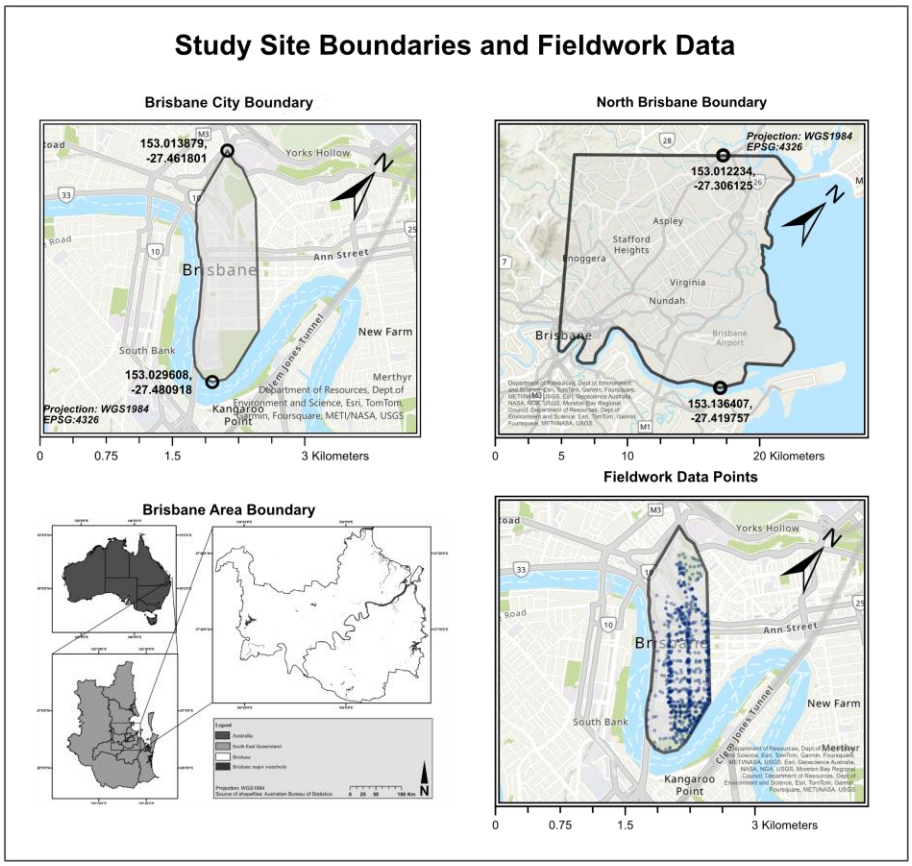

Figure 1. The collection of the boundaries surrounding all study sites measured and the fieldwork data points collected.

Note. Bottom-left map adapted from Modelling the urban heat island effect of smart growth policy scenarios in Brisbane [Case study area], by Deilami K & Kamruzzaman M, 2017*,* https://doi.org/10.1016/j.landusepol.2017.02.027

2.2 Fieldwork

Fieldwork took place over six days between 16/04/2024 and 26/04/2024. For each of these days, several groups or individuals were equipped with a HOBO U23 Pro v2 temperature and relative humidity data logger and an iPad with the Global Navigation Satellite System (GNSS) Groundsman for iOS installed. At intermittent coordinates, within the site boundaries (Figure 1) air temperature, surface cover, humidity, and lux values were recorded using the HOBO data logger and stored in the Groundsman application. GNSSs can be subject to interferences from atmospheric delays, multipath effects, satellite geometries and signal obstructions. To quantify the accuracy of the GNSS used, each group or individual recorded an initial point at a permanent survey marker (PSM). Xstd = ~5 m, Ystd = ~12.5 m, Area = 389 m (see Figure A1 in Appendix A).

2.3 Software and Analysis

2.3.1 Field Data Mapping and Computation

Field data was exported from the Groundsman application as a GeoJSON file to ArcGIS Pro 3.3; hereinafter referred to as ArcGIS. The data was manipulated using ArcGIS to generate an interpolated raster with the Empirical Bayesian Kriging tool to visually highlight any hotspots throughout the city boundary. Three sequential polygons overlaying Brisbane City were designated by the area's most prominent feature (i.e., botanical gardens). The Spatial Join tool was used to segregate the point data within the polygons and was then statistically evaluated by using the Optimized Hotspot Analysis tool. This analysis calculates the spatial autocorrelation

(Gi statistic) for each point and categorises them by 90, 95, and 99% confidence intervals against a null hypothesis distribution generated from the data.

2.3.2 Remote Sensing Mapping and Computation

The image sourced from Earth Explorer was provided as a raster with a 30-metre pixel resolution, imported into ArcGIS, and clipped to the boundaries using the Clip Raster tool. Values from the raster were converted to Celsius (see Appendix A, Figure A2). The raster was converted into point data using the Raster to Point tool and each point was assigned XY coordinates using the Add XY Coordinates tool. Data segregation and analysis was conducted using the same method outlined in Section 2.3.1, except the segregations were labelled ordinally from their distance to the city (i.e., Brisbane North 1, …).

2.3.3 Statistical Analysis of Average Temperature

LST and air temperature averages were compared to one another testing for a significant difference from a null hypothesis of homogeneous mean values. A One-way ANOVA test was used to investigate the difference of means, assuming that the data is independent and follows a normal distribution. The statistics-specific program ‘R’ was used to complete the ANOVA testing and to plot the averages for the remote sensing and experimental data. Note, the data provided for LSTs over North Brisbane was far too great in number and it was necessary that the raster be resampled to three times the original cell size, using the Resample tool in ArcGIS.

3. Results

3.1 Summary

Three different scales of LST were measured in the Brisbane area (Table 1). Of the three scales, the microscale for both the experimental and remote sensing data appeared to show

significant average temperature differences between the Roma Street Gardens, Brisbane City, and City Botanic Gardens. In contrast, the North Brisbane 2 and 3 regions displayed essentially no difference between average LSTs.

3.2 Remote Sensing Across Brisbane City

Figures 2 and 3 collectively demonstrate a clear difference in hot spot distribution between the three regions: Roma Street Gardens, Brisbane Central, and City Botanic Gardens. Of these regions, Brisbane Central contained the highest percentage of hot spot instances at a 99% confidence interval (CI) (41.5%, ~27.2°C - 31.1°C) with homogeneity presenting at a moderate 23.33%. The Roma Street Gardens region shared similarities with Brisbane Central at a 99% CI hot spot distribution of 32.6% and 30.5% homogeneity. The City Botanic Gardens region was predictably almost exclusively a 99% CI cold spot (89.1%, 22.5°C - 27.2°C).

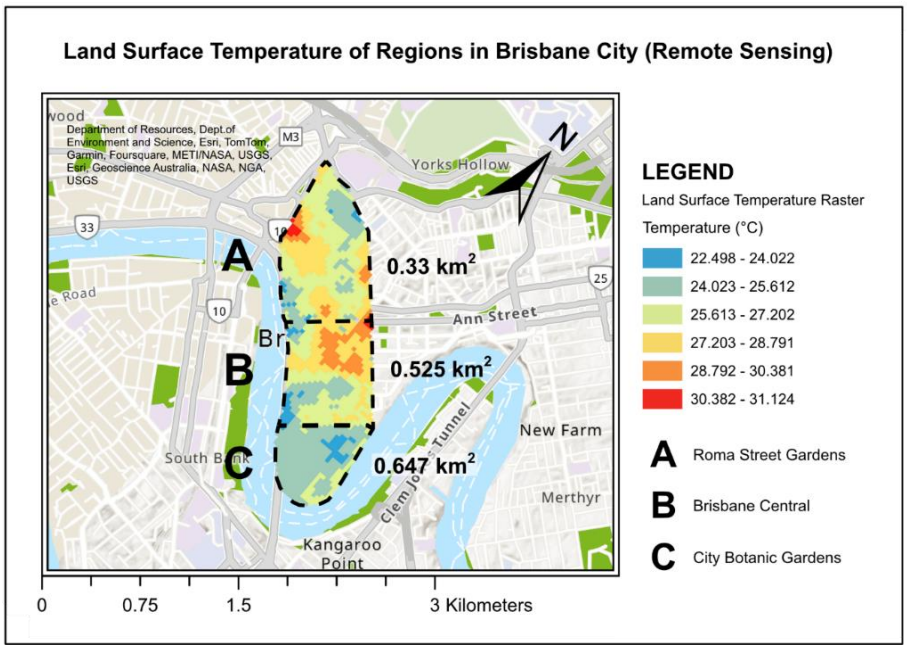

Figure 2. A 30-metre pixel resolution raster overlaying Brisbane City, displaying the LST variations between the three regions: Roma Street Gardens, Brisbane Central, and City Botanic Gardens.

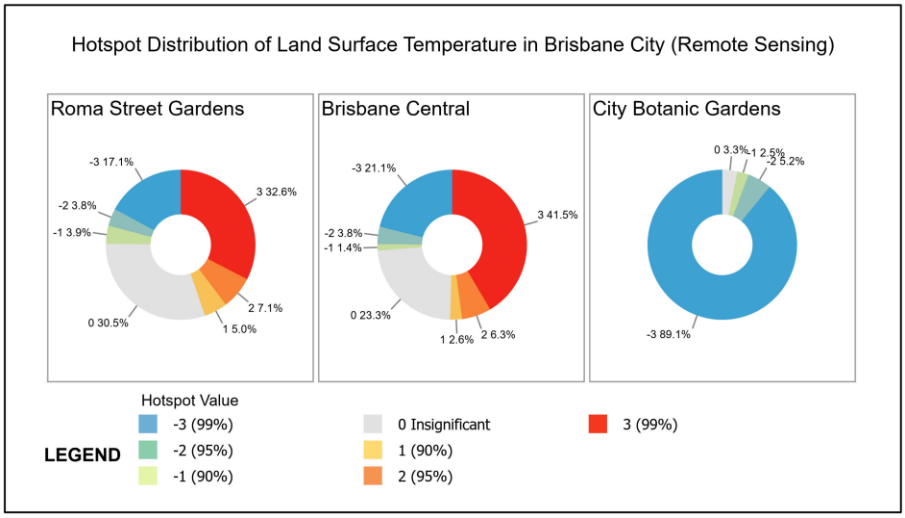

Figure 3. A hotspot distribution chart of a 30-metre pixel raster overlaying Brisbane City defined by 90, 95 and 99% confidence intervals.

3.3 Experimental Data Across Brisbane City

Figures 4 and 5 collectively show a clear difference in air temperatures experimentally collected across the regions also graphed in Figure 2. The most striking result from the experimental data, was the 99% CI hot spot distribution within the Roma Street Gardens region (50.5%, ~25.5°C - 27°C), accompanied by a total insignificance of 31.8%. Brisbane Central showed little evidence of hot spots, a minor presence of cold spots (31.07%, 22.8°C - 24.9°C) and primarily showed an insignificant difference in air temperature (46.9%). Despite Brisbane Central being mostly unremarkable, an anomalous cold spot with a temperature several bins lower than its nearest neighbours (~22.8°C - 23.4°C) was recorded. The City Botanic Gardens showed minor variation from its counterpart in Figure 3 with a dominant cold spot (71.8%, ~22.8°C - 24.9°C).

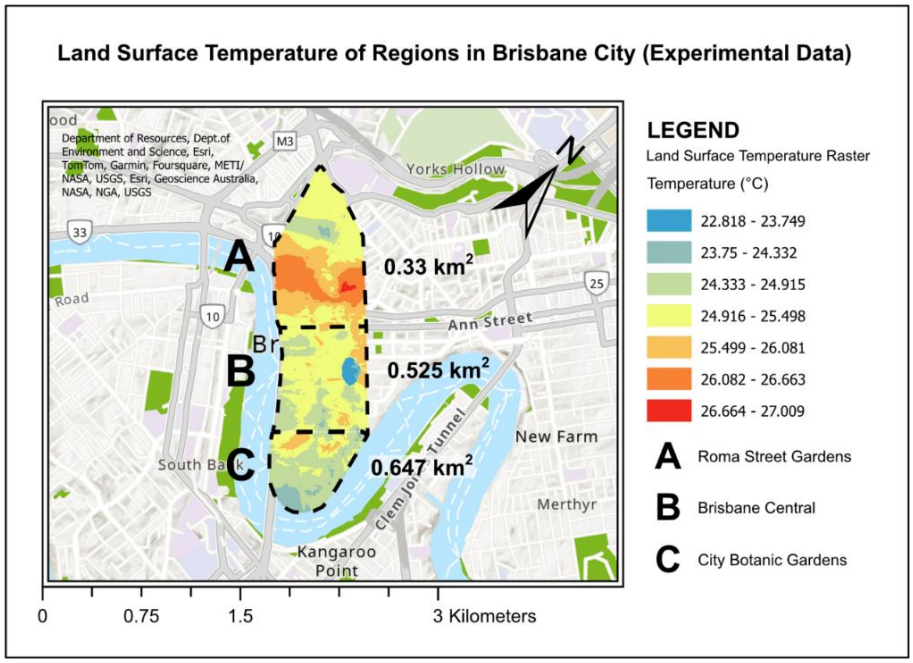

Figure 4. A high-resolution Empirical Bayesian Kriging raster overlaying Brisbane City, displaying the LST variations between the three regions: Roma Street Gardens, Brisbane Central, and City Botanic Gardens.

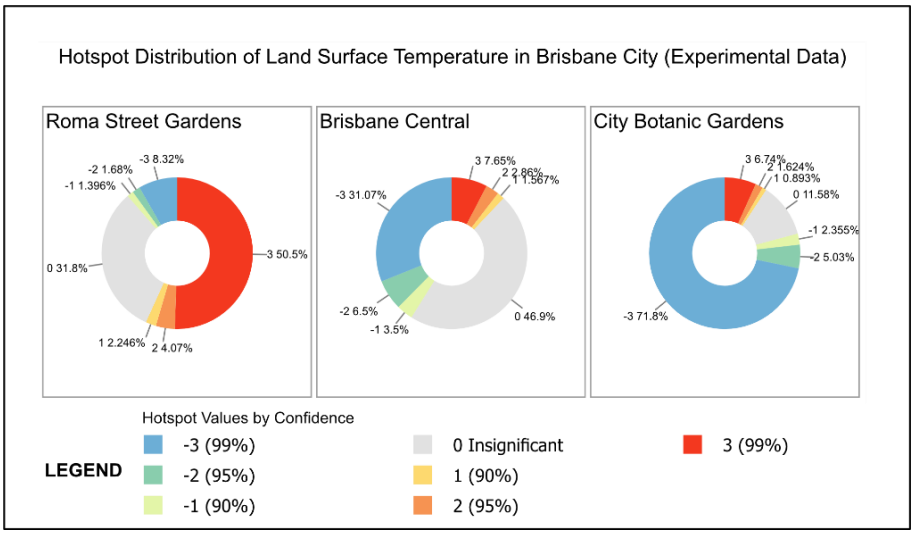

Figure 5. A hotspot distribution chart of experimental data collected across Brisbane City defined by 90, 95 and 99% confidence intervals.

3.4 Remote Sensing Across North Brisbane

The hot spot distribution across North Brisbane displayed in figures 6 and 7 show extremely similar results across all regions. The 99% CI hotspot distributions for Brisbane North 1, 2 and 3 showed a maximum difference of 6%, (36%, 30% and 35.4%) respectively. The cold spots were observed at a similar maximum difference of 9.2% (24.1%, 30.4% and 33.3%) and insignificance showing as 27.6%, 27.9% and 21.2%.

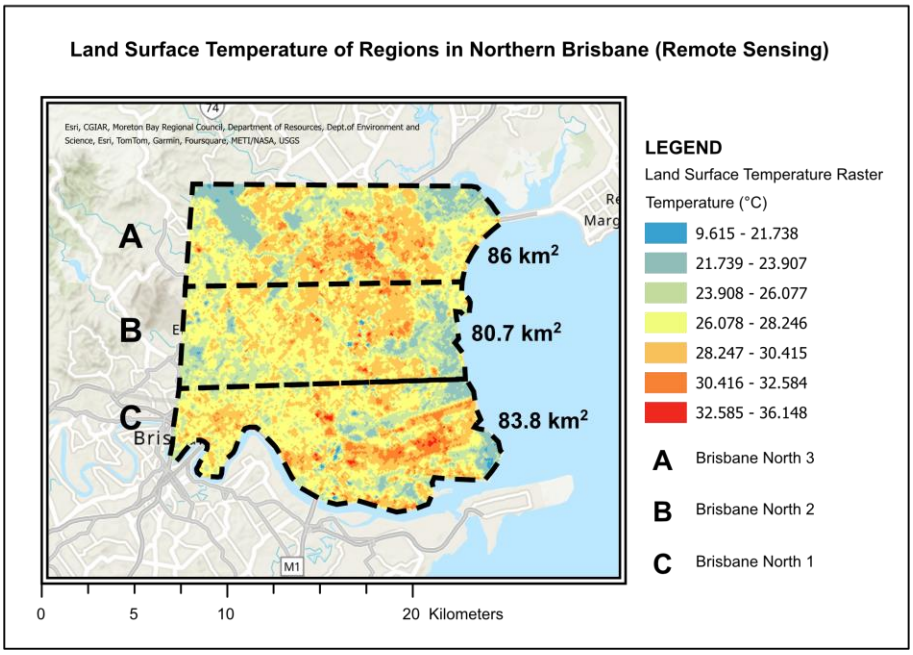

Figure 6. A 30-metre pixel resolution raster overlaying North Brisbane, displaying the LST variations between the three regions: Brisbane North 1, Brisbane North 2, and Brisbane North 3.

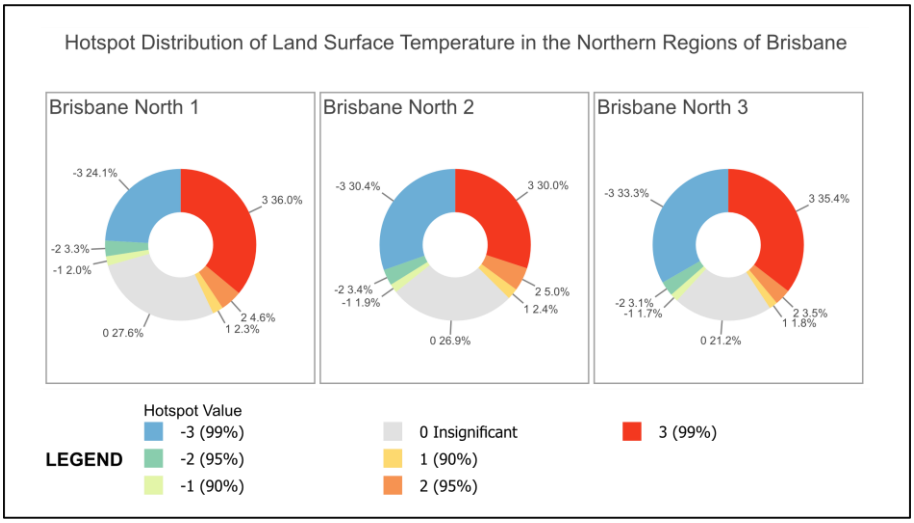

Figure 7. A hotspot distribution chart of experimental data collected across North Brisbane defined by 90, 95 and 99% confidence intervals.

3.5 Regional Averages

Remotely sensed LST data over Brisbane City showed a maximum difference of 2.1°C. North Brisbane remote sensing showed the same average temperatures for Brisbane North 2 and 3 (26.5°C), as compared to Brisbane North 1 which was 0.4°C warmer (26.9°C). The experimental data marked a 0.7°C maximum difference (24.9°C – 25.6°C). All regions within each dataset displayed a significant difference from equal means (Table 2).

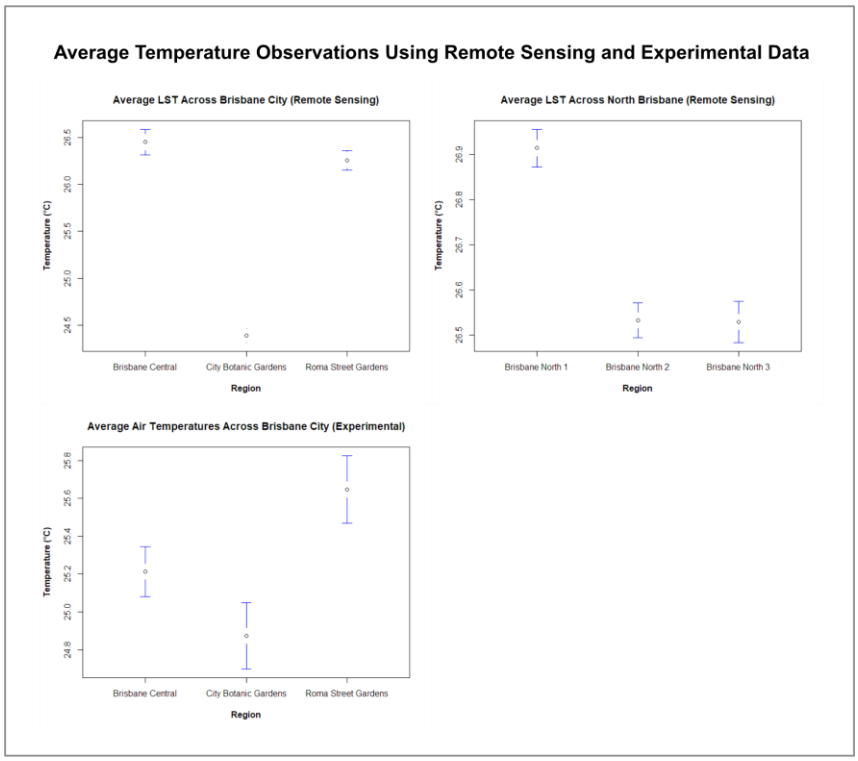

Figure 8. Average temperature differences among regions in the Brisbane City and North Brisbane area, including experimental data for Brisbane City.

ANOVA Results	**DF**	**Sum of Squares**	**F value**	**P value**
North Brisbane (Remote Sensing)	2	1027	107.9	$<2e^{-16}$
Brisbane City (Remote Sensing)	2	1102	280.9	$<2e^{-16}$
Brisbane City (Experimental)	2	70.8	19.1	$7.62e^{-9}$

Table 2. A results table for One-way ANOVA tests conducted on the average air and land surface temperatures measured for Brisbane City and North Brisbane areas.

4. Discussion

The hypothesis suggested that different scales significantly impact the measurement of contributing UHI factors, and that experimental data provides valuable insights compared to remote sensing. The analyses for hot spot distributions and average temperature differences

indicated the suitability of data at varying scales, but also highlighted the need for robust measurement techniques due to limitations in analytical methods and the experimental data.

4.1 Microscale

Differences between remote sensing and experimental data on a microscale revealed important considerations. Experimental data contradicted remote sensing, particularly in Brisbane Central and Roma Street Gardens, showing more homogenous temperatures and pronounced hot spots, respectively. These contradictions suggest low-resolution imagery may overgeneralize factors like public transport, building densities, and air flow (Lin et al., 2017; Yang & Li, 2013). As an example of high-resolution imagery, Saaroni et al. (2000) used a thermal video radiometer mounted to a helicopter at an altitude of 2000 m to measure surface temperatures of Tel-Aviv, Israel. Their results indicated clear temperature rises between object surfaces, with surface temperatures rising by more than 10°C and air temperatures by 5.6°C. Similarly, within this study, the experimental data was able to detect discrepancies in Roma Street Gardens far more accurately than the sourced imagery. Green areas like Roma Street Gardens are typically known to reduce UHI factor intensities (Thom et al., 2016), however, it was found that the gardens were experiencing the opposite effect, most likely due to an adjacent train line detectable only through atmospheric, in-person measurements. Examples such as this emphasize the value of experimental data on a microscale and how low-resolution satellite imagery may cause misinterpretations.

4.2 Mesoscale

At the mesoscale, satellite data showed visually similar results with a significant yet miniscule statistical difference, indicating no significant relationship with UHIs. This would suggest that the mesoscale is unsuitable for detecting UHI factors. However, a study by

Varentsov (2021) argues the factors contributing to UHIs on a mesoscale are primarily due to land cover types, wind movements, and climate changes, none of which were considered in this study. Thus, the mesoscale analysis in this study is of weak veracity.

4.3 Macroscale

As the current technology used in this study was unsuitable, an adjacent study that considers the greater Brisbane area will be referenced as proof of macroscale suitability (Deilami & Kamruzzaman, 2017). Deilami and Kamruzzaman measured UHI intensity changes externally collected over 22 years using Landsat imagery, finding that UHI intensity measurements at a macroscale are resilient to weather conditions and primarily influenced by anthropogenic activities (see Figure A3 in Appendix A). Therefore, satellite imagery is suitable for analyzing UHI factors at this scale as weather events and local anomalies become negligible over time.

4.4 Limitations and Suggestions

Experimental data produced an anomalous cold spot in central Brisbane, likely due to data error but too small to be considered an outlier. This emphasizes the need for more frequent testing to accommodate simple errors. The study also suffered from a lack of processing power for large datasets, suggesting computational power should be prioritized in future studies. Lastly, the mesoscale was poorly represented in this report as temporal nor climatic factors were considered. It is recommended that any studies investigating UHIs larger than a microscale include temporal variations as a key factor.

5. Conclusion

Determining scale is a major consideration for UHI analysis, it is highly dependent on the scope of the study. Microscale UHI contributors were effectively quantified through spatial and statistical analyses from both an experimental and remote perspective. However, the mesoscale

was poorly represented due to the lack of important inclusions such as climate shifts and temporal variations, and evidence for the macroscale proved to be the most resilient to low-resolution imagery. When undertaking a geospatial study, the scale and type of data collection is the most important consideration and should be decided upon first and foremost.

6. References

Deilami, K., & Kamruzzaman, Md. (2017). Modelling the urban heat island effect of smart growth policy scenarios in Brisbane. *Land Use Policy*, *64*, 38–55. https://doi.org/10.1016/j.landusepol.2017.02.027

Giannaros, C., Nenes, A., Giannaros, T. M., Kourtidis, K., & Melas, D. (2018). A comprehensive approach for the simulation of the Urban Heat Island effect with the WRF/SLUCM modeling system: The case of Athens (Greece). *Atmospheric Research*, *201*, 86–101. https://doi.org/10.1016/j.atmosres.2017.10.015

Kim, S. W., & Brown, R. D. (2021). Urban heat island (UHI) intensity and magnitude estimations: A systematic literature review. *Science of The Total Environment*, *779*, 146389. https://doi.org/10.1016/j.scitotenv.2021.146389

Li, H., Zhou, Y., Li, X., Meng, L., Wang, X., Wu, S., & Sodoudi, S. (2018). A new method to quantify surface urban heat island intensity. *Science of The Total Environment*, *624*, 262–272. https://doi.org/10.1016/j.scitotenv.2017.11.360

Lin, P., Lau, S. S. Y., Qin, H., & Gou, Z. (2017). Effects of urban planning indicators on urban heat island: a case study of pocket parks in high-rise high-density environment. *Landscape and Urban Planning*, *168*, 48–60. https://doi.org/10.1016/j.landurbplan.2017.09.024

Saaroni, H., Ben-Dor, E., Bitan, A., & Potchter, O. (2000). Spatial distribution and microscale characteristics of the urban heat island in Tel-Aviv, Israel. *Landscape and Urban Planning*, *48*(1–2), 1–18. https://doi.org/10.1016/S0169-2046(99)00075-4

Thom, J. K., Coutts, A. M., Broadbent, A. M., & Tapper, N. J. (2016). The influence of increasing tree cover on mean radiant temperature across a mixed development suburb in Adelaide, Australia. *Urban Forestry & Urban Greening*, *20*, 233–242. https://doi.org/10.1016/j.ufug.2016.08.016

Varentsov, M., Fenner, D., Meier, F., Samsonov, T., & Demuzere, M. (2021). Quantifying Local and Mesoscale Drivers of the Urban Heat Island of Moscow with Reference and Crowdsourced Observations. *Frontiers in Environmental Science*, *9*. https://doi.org/10.3389/fenvs.2021.716968

Yang, X., & Li, Y. (2013). Development of a Three-Dimensional Urban Energy Model for Predicting and Understanding Surface Temperature Distribution. *Boundary-Layer Meteorology*, *149*, 303–321.

7. Appendix A

Note: *I was unable to collect the Week 7 group data as I was absent, I only had access to Week 8 group data.*

Table A1 Group Field Dataset:

Description:

This dataset was collected by a group of students within the EVB203 class from the Queensland University of Technology (QUT). Measurements included: air temperature, surface

cover, humidity, and lux values, between 16/04/2024 and 26/04/2024. Data was gathered using HOBO U23 Pro v2 data loggers and iPads with the GNSS Groundsman app for iOS.

Variable	Description
Date	Date of data collection. Format is DD/MM/YYYY.
Time	Timestamp of data collection. 24-hour time.
Latitude	Collected using the Groundsman application for iOS. Units are degrees (°). [GCS_WGS_1984]
Longitude	Collected using the Groundsman application for iOS. Units are degrees (°). [GCS_WGS_1984]
Light	Collected using the provided iPad and input into the Groundsman application. Units are lux (lx).
Surface Cover	Collected *via* visual inspection and inputted into the Groundsman application.
Author	QUT student username of the individual inputting data
Air Temperature	Collected using the HOBO data logger and input into the Groundsman application. Units are (°C).
Humidity	Collected using the HOBO data logger and input into the Groundsman application. Units are (%).

Time	Light (lx)	Surface Cover	Date	Author	Air Temperature (°C)	Humidity (%)	Latitude	Longitude
9:42	1471	Concrete	24/04/2024	n11601311	23.914	64.811	-27.4741	153.0265
9:39	1508	Concrete	24/04/2024	n11601311	23.871	66.349	-27.4741	153.0265
9:43	1471	Concrete	24/04/2024	n11601311	23.871	65.031	-27.4734	153.0254
9:46	1269	Concrete	24/04/2024	n11601311	23.914	65.201	-27.4734	153.0256
9:49	623	Canopy	24/04/2024	n11601311	24.214	64.005	-27.4717	153.0245
9:53	796	Concrete	24/04/2024	n11601311	24.429	63.028	-27.4712	153.0235
9:55	1355	Concrete	24/04/2024	n11601311	24.429	62.979	-27.4704	153.0228
9:58	1724	Concrete	24/04/2024	n11601311	24.3	63.394	-27.4697	153.0223
10:01	1444	Concrete	24/04/2024	n11601311	24.214	63.883	-27.4691	153.021

10:03	8404	Concrete	24/04/2024	n11601311	24.343	64.591	-27.468	153.0205
10:13	6412	Concrete	24/04/2024	n11601311	25.244	61.587	-27.4669	153.0201
10:16	6506	Concrete	24/04/2024	n11601311	26.102	60.928	-27.467	153.0214
10:18	19208	Concrete	24/04/2024	n11601311	26.574	57.973	-27.4673	153.0212
10:22	10466	Concrete	24/04/2024	n11601311	27.132	56.117	-27.4686	153.023
10:28	3662	Concrete	24/04/2024	n11601311	26.703	60.781	-27.467	153.0252
10:30	1370	Concrete	24/04/2024	n11601311	26.703	57.973	-27.4669	153.0252
10:33	2071	Concrete	24/04/2024	n11601311	26.531	58.193	-27.4681	153.0269
10:35	2391	Concrete	24/04/2024	n11601311	26.274	59.756	-27.468	153.0272
10:38	8682	Concrete	24/04/2024	n11601311	26.746	58.95	-27.4694	153.0277
10:39	7552	Canopy	24/04/2024	n11601311	27.175	57.778	-27.4703	153.0301
10:42	4167	Concrete	24/04/2024	n11601311	27.432	55.311	-27.4711	153.0298
10:44	11427	Concrete	24/04/2024	n11601311	26.874	58.779	-27.472	153.0307
10:47	797	Canopy	24/04/2024	n11601311	26.874	57.9	-27.4734	153.0309
10:50	1314	Canopy	24/04/2024	n11601311	26.274	61.05	-27.4745	153.0312
10:53	2397	Canopy	24/04/2024	n11601311	25.845	62.93	-27.4757	153.0315
10:56	960	Canopy	24/04/2024	n11601311	25.973	62.198	-27.4769	153.0316
10:59	48	Canopy	24/04/2024	n11601311	25.587	65.934	-27.4777	153.031
11:01	1542	Canopy	24/04/2024	n11601311	25.287	64.371	-27.4773	153.0305
11:03	1682	Canopy	24/04/2024	n11601311	25.416	62.002	-27.4781	153.0298
11:05	2592	Concrete	24/04/2024	n11601311	25.459	62.613	-27.4785	153.0292

Table A2 Class Field Dataset:

Description:

This dataset was collected by the EVB203 class from the Queensland University of Technology (QUT). Measurements included: air temperature, surface cover, humidity, and lux

values, between 16/04/2024 and 26/04/2024. Data was gathered using HOBO U23 Pro v2 data loggers and iPads with the GNSS Groundsman app for iOS.

Variable	Description
Date	Date of data collection. Format is DD/MM/YYYY.
Time	Timestamp of data collection. 24-hour time.
Latitude	Collected using the Groundsman application for iOS. Units are degrees (°). [GCS_WGS_1984]
Longitude	Collected using the Groundsman application for iOS. Units are degrees (°). [GCS_WGS_1984]
Light	Collected using the provided iPad and input into the Groundsman application. Units are lux (lx).
Surface Cover	Collected *via* visual inspection and inputted into the Groundsman application.
Author	QUT student username of the individual inputting data
Air Temperature	Collected using the HOBO data logger and input into the Groundsman application. Units are (°C).
Humidity	Collected using the HOBO data logger and input into the Groundsman application. Units are (%).

Time	Light	Surface Cover	Date	Author	Air Temperature (°C)	Humidity (%)	Latitude	Longitude
10:08	38543	Grass	24/04/2024	n10689079	26.280	61.854	153.021	-27.468
10:10	2146	Canopy	24/04/2024	n10689079	26.451	61.973	153.0211	-27.4675
10:12	41084	Concrete	24/04/2024	n10689079	26.916	59.853	153.0211	-27.4674
10:58	3131	Canopy	24/04/2024	n10689079	28.468	60.063	153.0224	-27.4654
11:02	1854	Canopy	24/04/2024	n10689079	27.604	60.301	153.0217	-27.4659
11:07	19070	Concrete	24/04/2024	n10689079	27.825	61.453	153.0233	-27.4676
11:09	12518	Concrete	24/04/2024	n10689079	27.948	58.110	153.0238	-27.4682
11:09	2035	Concrete	24/04/2024	n10689079	27.948	58.110	153.0244	-27.4721
9:50	42725	Concrete	24/04/2024	n10689079	23.569	69.638	153.024	-27.4724
9:48	46263	Grass	24/04/2024	n10689079	23.063	70.049	153.0239	-27.4721

...	...	...	...	...	...	...	...	...

Note: This is a subset of the dataset. The full dataset includes additional measurements and is available upon request.

Figure A1 Permanent Survey Marker:

Spatial Distribution of Permanent Survey Markers with a 1 Standard Deviation Ellipse

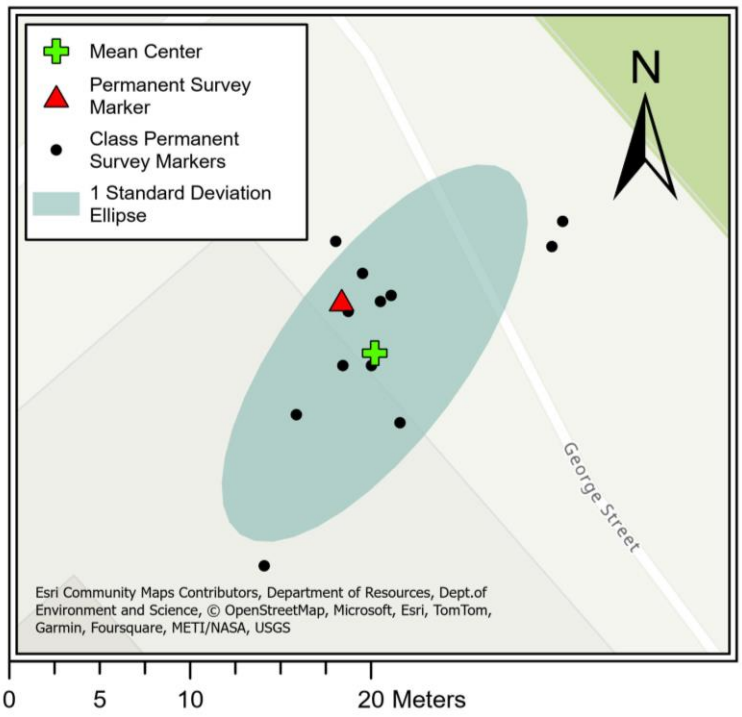

Description:

This map shows the spatial distribution of class permanent survey markers (black dots). The red triangle represents the permanent survey marker (PSM), and the green cross denotes the mean center of these markers. The light blue ellipse indicates the 1 standard deviation area around the mean center, illustrating the spatial variability of the survey markers.

Figure A2 Additional Dataset:

Land Surface Temperature Large Scale Remotely Sensed Satellite Raster

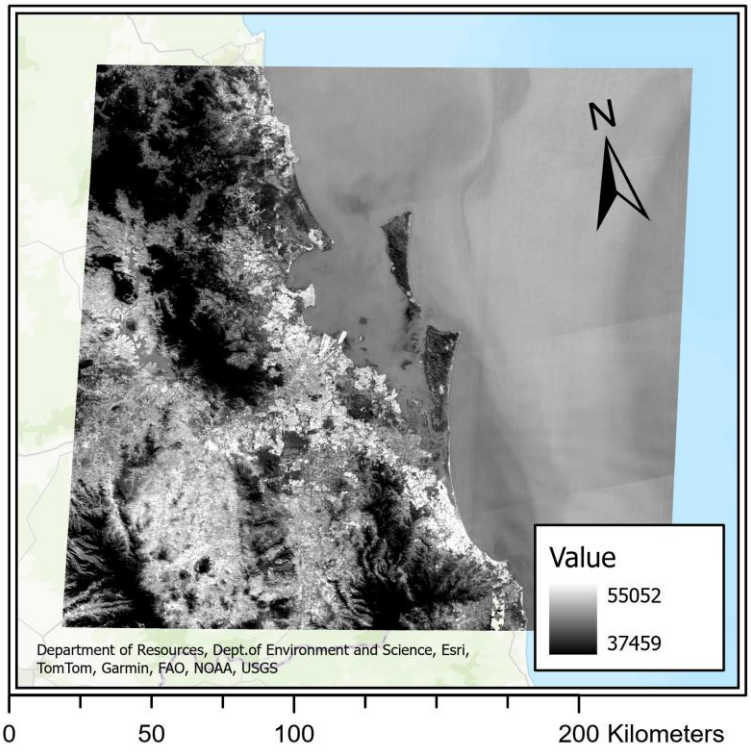

Description:

This map shows the spatial distribution of LST on 09/04/2024 over Southeast Queensland closer to the shoreline. Collected from the public website Earth Explorer, which provides access to images in the Landsat 8-9 OLI/TIRS C2 L2 dataset. The values given to the greyscale cells indicate the raw LST data collected, and is converted to Kelvin, then Degrees Celsius with the equations:

$$K = cell\ value \times 0.00341802 + 149.0 \qquad °C = K - 273.15$$

Table A3 Additional Dataset:

Description:

This table was created in ArcGIS from data associated with each pixel of the raster provided by the Landsat program. Measurements included: Temperature, Latitude and Longitude on 09/04/2024.

Variable	Description
Land Surface Temperature	Calculated from the raster provided by the Landsat 8-9 OLI/TIRS C2 L2 dataset. Units are degrees Celsius °C.
Latitude	Developed from the raster provided by the Landsat 8-9 OLI/TIRS C2 L2 dataset. Units are degrees (°). [GCS_WGS_1984]
Longitude	Developed from the raster provided by the Landsat 8-9 OLI/TIRS C2 L2 dataset. Units are degrees (°). [GCS_WGS_1984]

Land Surface Temperature (°C)	Latitude	Longitude
23	153.041933	-27.281182
23	153.042236	-27.281181
23	153.042539	-27.281181
23	153.042842	-27.281181
23	153.043146	-27.281181
23	153.043449	-27.281181
23	153.043752	-27.281181
23	153.044055	-27.281181
23	153.044358	-27.281181
23	153.044661	-27.281181
…	…	…

Note: This is a subset of the dataset. The full dataset includes additional measurements and is available upon request.

Figure A3 Macroscale Temporal Variation

Spatial patterns of the UHI intensities in Brisbane

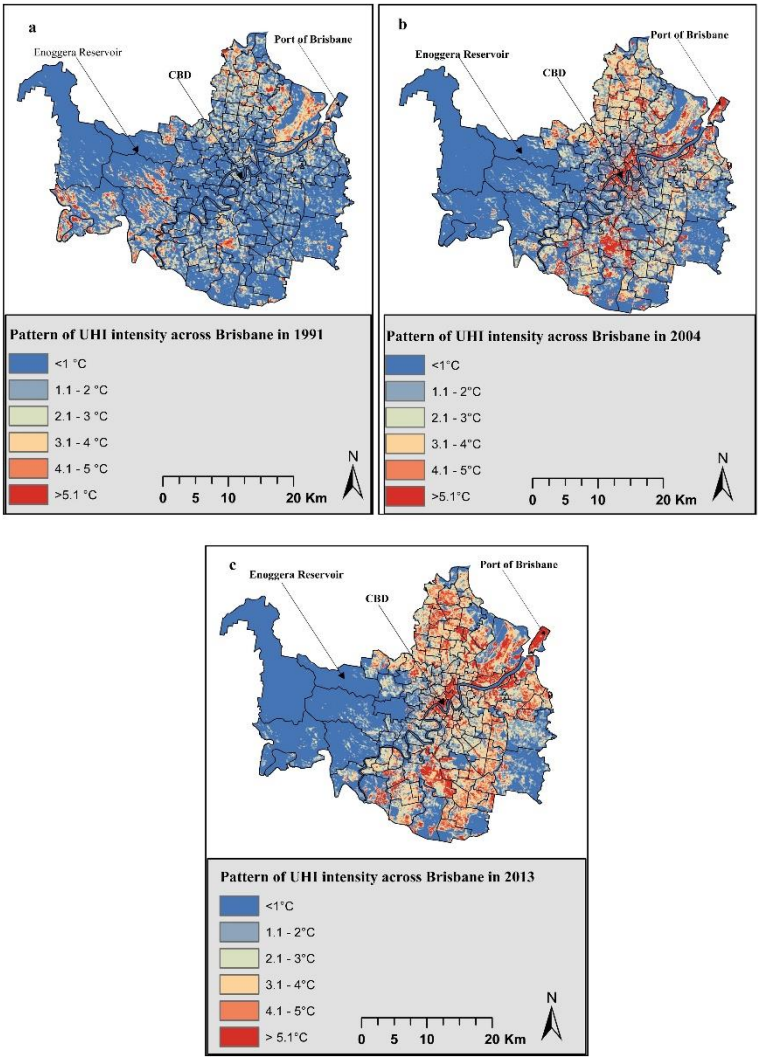

Description:

This map shows the spatial pattern of UHI intensities in Brisbane from 1991 to 2013. Measurements were taken in reference to surrounding rural areas. Adapted from Deilami and Kamruzzaman, (2017).